J. Fluid Mech. (2025), *vol.* 1018, A29, doi:10.1017/jfm.2025.10531

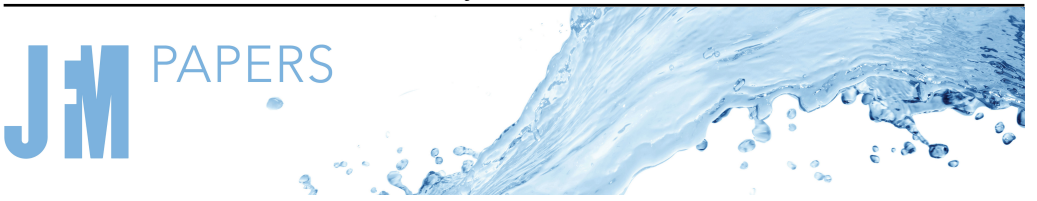

On transients in displacement ventilation

Daniel A. Toy[1] **and Andrew W. Woods**[1]

[1]Institute for Energy and Environmental Flows, University of Cambridge, Madingley Road, Cambridge CB3 0EZ, UK

Corresponding author: Andrew W. Woods, andy@bpi.cam.ac.uk

(Received 4 January 2025; revised 20 May 2025; accepted 25 June 2025)

A series of new laboratory experiments explore the transient flow in an enclosed space of depth H, which is subject to an upward displacement ventilation flux, Q_V, and which contains a localised heat source of buoyancy flux F_s, when the buoyancy of the ventilation air changes by $\Delta g'$. Initially, the plume, produced by the heat source, entrains the ventilation air, leading to a two-layer stratification which depends on the dimensionless strength of convection, $\mu \propto F_s^{1/3} H^{5/3}/Q_V$. When the buoyancy of the ventilation air decreases, $\Delta g' < 0$, a new layer of relatively dense fluid grows next to the floor. The fluid entrained by the plume from this new layer causes the plume to intrude between the original upper and lower layers. For a sufficiently large decrease in buoyancy, $|\Delta g' Q_V/F_s| > 1$, then as the new lower layer grows, the plume eventually becomes negatively buoyant relative to the original lower layer and intrudes between the new lowest layer and the original lower layer. When the buoyancy of the air supply increases, $\Delta g' > 0$, it mixes with the fluid in the original lower layer. If the increase in buoyancy is sufficient, $\Delta g' Q_V/F_s > 1$, then the new supply air eventually also mixes with the original upper layer. In each case, a new two-layer stratification becomes re-established. We propose new models for the evolution of the transient flow, assuming that the buoyancy profile can be approximated by a staircase of well-mixed layers. These layers are emptied or filled through the action of the plume and ventilation. We find that the model predictions are consistent with our new experiments in each of the four regimes. We conclude by discussing the implications of these transient flows for thermal comfort and the mixing of contaminants into the occupied lower region of the space.

Key words: turbulent mixing, plumes/thermals, convection in cavities

1. Introduction

Buildings require ventilation to supply fresh air and so ensure contaminants and heat do not accumulate. Broadly, ventilation can be divided into two categories: mixing and

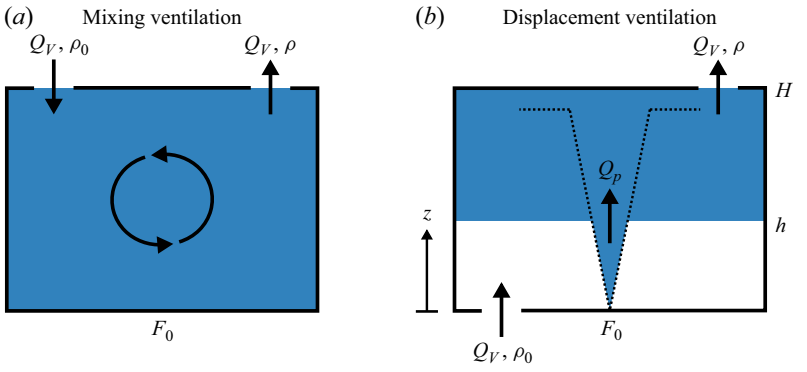

Figure 1. Schematic illustrating the types of ventilation. The ventilation volume flux is Q_V, ρ is the density and F_0 is the buoyancy flux from internal heat sources.

displacement ventilation (Linden 1999). In a mixing system, the incoming air rapidly mixes with the air already in the space, leading to a relatively uniform temperature and contaminant distribution. One method for implementing this kind of ventilation is to supply and extract air at a high level. Typically, internal heat sources warm the air, so if the incoming air is relatively cool and dense, it will spontaneously mix (figure 1*a*).

In contrast, displacement ventilation systems supply air near the floor and extract air close to the ceiling. Internal heat sources lead to turbulent buoyant plumes rising through the space. The interaction between the plumes and the upward ventilation can generate a stable density interface between a warm upper layer and cooler lower layer (Linden, Lane-Serff & Smeed 1990) (figure 1*b*). In well-designed displacement ventilation, the interface between the layers is located above the occupied zone; the occupants are surrounded by fresh supply air while contaminants and excess heat are transported into the upper layer by the plumes. As a result, displacement ventilation can offer significant advantages over mixing ventilation because less cooling work is required and the occupants are exposed to fewer contaminants than in mixing ventilation.

Previous studies on the fluid mechanics of displacement ventilation have focused on naturally ventilated buildings, including the analysis of the steady state (Linden *et al.* 1990) and the transient evolution of the flow to steady state resulting from a change in the heat sources (Kaye & Hunt 2004; Bower *et al.* 2008; Fitzgerald & Woods 2010). The model and experiments presented by Bower *et al.* (2008) illustrated the transient evolution when there is an increase or decrease in the buoyancy flux of the point-source plume issuing from the floor of the room. For reference, in steady state, the upper layer has the same buoyancy as the plume once it reaches the interface (Linden *et al.* 1990). With an increase in buoyancy flux, the plume rises to the ceiling. The continuing plume then entrains the original upper layer, while the new upper layer develops from the ceiling and gradually descends to the depth of the original upper layer, once the original upper-layer fluid has been entrained by the plume. In the case of a decrease in the buoyancy flux, the plume intrudes at the interface to form a new layer, while the original upper layer ventilates from the space, re-establishing the two-layer stratification. Fitzgerald & Woods (2007) considered the change in a naturally ventilated displacement flow in the case in which the buoyancy is supplied from an areal source. In that case, in steady state, the air in the interior is well mixed and ventilates from the space. A decrease in the buoyancy flux leads to the formation of a new denser lower layer, which gradually rises through the space as the original, more buoyant, layer ventilates from the top of the space. In contrast, an increase in the buoyancy flux

leads to transient mixing across the whole depth of the room until the interior buoyancy has increased to the new steady-state value.

Other studies have explored contaminant transport in a steady flow (Hunt & Kaye 2006; Bolster & Linden 2007; Bolster & Caulfield 2008). However, most buildings are mechanically ventilated, and this leads to some important differences in the flow (Toy & Woods 2025). Lin & Linden (2005*a*), Liu & Linden (2006) and Alajmi & El-Amer (2010) showed that a two-layer system is still established but, as Toy & Woods (2025) demonstrate, decoupling the ventilation volume flux from the thermal stratification in the room means it is possible to over- or under-ventilate the system relative to the volume flux of the natural convection produced by the heat sources. In the idealised situation in which the heat source is modelled as a point source, this transition in behaviour is described by the parameter

$$\mu = \frac{\lambda F_s^{1/3} H^{5/3}}{Q_V}, \tag{1.1}$$

which represents the ratio of the volume flux in the plumes at the ceiling to the ventilation volume flux, πQ_V. Here, $\lambda = (6\alpha/5)(9\alpha/10)^{1/3}$ is an empirical constant related to the entrainment coefficient α (Morton, Taylor & Turner 1956), πF_s is the buoyancy flux produced by the heat source and H is the height of the room (we note that the factor of $\pi \approx 3.14$ in these definitions is chosen to simplify the form of the plume equations and their solutions; see § 4.1).

Provided that the volume flux in the plumes exceeds the ventilation volume flux sufficiently, the system is under-ventilated and, for $\mu \gtrsim 2$, it is reasonable to ignore the turbulence of the plumes on the dynamics of the upper layer (Toy & Woods 2025). In this case, in steady state, there is a depth, h, at which the volume flux in the plumes matches the ventilation. Here, the vertical velocity in the fluid outside the plume is zero and an interface forms between the upper and lower layers (Baines & Turner 1969; Linden *et al.* 1990). The height of the interface is given by

$$\frac{h}{H} = \mu^{-3/5}. \tag{1.2}$$

The temperature of the upper layer, T_u, can be calculated using an energy balance:

$$T_u = T_l + \frac{F_s}{g\beta Q_V}, \tag{1.3}$$

where T_l is the temperature of the air supply to the lower layer, g is the acceleration due to gravity and β is the coefficient of thermal expansion. For convenience in this paper, we express the air temperature T as a buoyancy, g', relative to the supply air in the initial steady state where under the Boussinesq approximation

$$g'(T) = g\frac{\rho_{l,0} - \rho}{\rho_{l,0}} = g\beta\left(T - T_{l,0}\right). \tag{1.4}$$

Rewriting (1.3) in terms of the buoyancy of the layers, we obtain

$$g'_u = g'_l + \frac{F_s}{Q_V}. \tag{1.5}$$

Typically, in mechanically ventilated spaces, the incoming air is tempered by passing through a heat exchanger before it enters the room. Occupants can then adjust the temperature and flow rate of the supply air. In some cases, the time scale of this adjustment

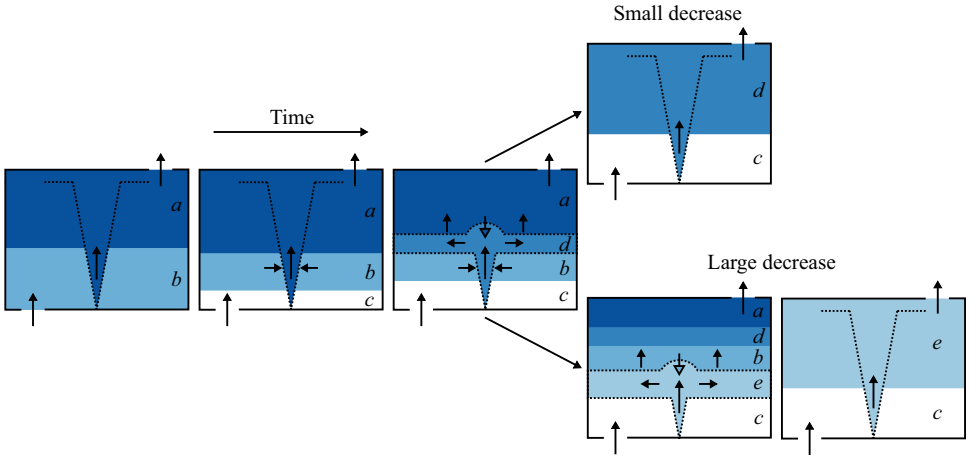

Figure 2. Schematic representation of the transient flow evolution following a rapid decrease in the buoyancy of the supply fluid. The shade of blue indicates the average buoyancy of the fluid in each layer. Dark blue has the largest buoyancy, and white has the smallest.

of the temperature may be slow compared with the ventilation time scale which is given by $T_V = AH/Q_V$, where πA is the cross-sectional area of the room, and the system will evolve through a series of quasi-steady states (1.2) and (1.5). Alternatively, in other situations, the variation may be much faster. These rapid changes can cause significant transient fluctuations in the air-flow dynamics, with profound implications for mixing and hence the air quality in the occupied zone during the transients.

In this paper, we consider the idealised case in which there is a step change in the supply temperature of the ventilation air, with a fixed ventilation rate, to develop insight into the effect of rapid changes. Following a step change to the air supply temperature, we identify four new transient flow regimes depending on whether the supply air is heated or cooled and on the magnitude of this temperature change.

Figure 2 shows a schematic of the transient flows when the temperature of the supply air decreases. Initially, there is a two-layer stratification (layers a and b), and the relatively cold supply fills a new layer (c) next to the floor. Fluid from this layer is entrained by the plume, which becomes less buoyant and forms an intrusion (d) between the original layers. If the decrease is small, this intrusion grows and replaces the original upper layer (a) while the original lower layer (b) is entrained by the plume. However, if the decrease is large, the plume may switch to form a new intrusion (e) below the original lower layer, which grows, eventually replacing the higher layers as they ventilate out of the space.

Figure 3 shows a schematic of the transient flows when the temperature of the supply air increases. The warm air supply mixes with the fluid in the lower layer (b). Fluid from this layer is entrained by the plume which becomes more buoyant and stratifies the region close to the ceiling (c). If the increase is small, the stratified layer descends and replaces the original upper layer (a) which is entrained by the plume. Otherwise, if the increase is large, both original layers can overturn and mix ($a + b$) until, eventually, the plume re-establishes a two-layer stratification.

To explore these different transient flows, the structure of this paper is as follows. In § 2 we describe our experimental model for variations in the supply air temperature. Then, in § 3, we describe the different flow regimes in detail. We develop a regime diagram in § 5 and propose new models for the evolution of the flow for the cases where the supply

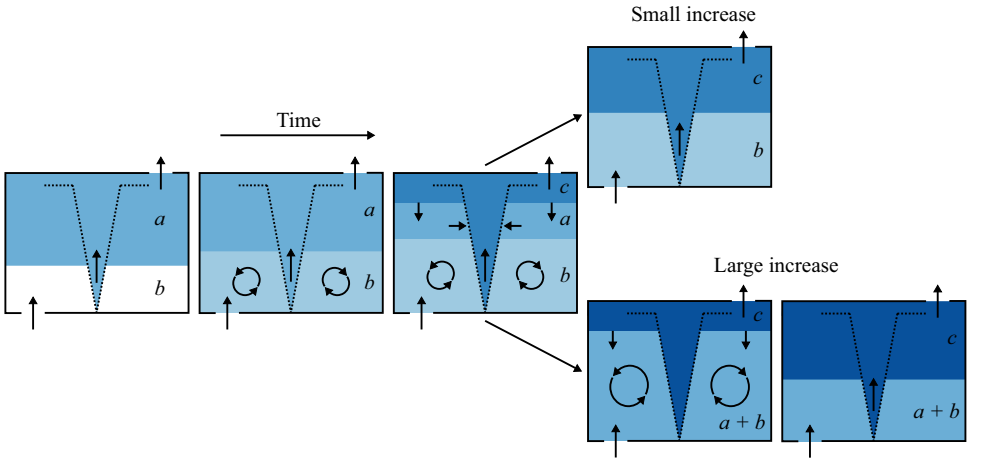

Figure 3. Schematic representation of the transient flow evolution following a rapid increase in the buoyancy of the supply fluid. The shade of blue indicates the average buoyancy of the fluid in each layer. Dark blue has the largest buoyancy, and white has the smallest.

air is cooled (§ 6) and heated (§ 7). Finally, we discuss our results in § 8 and draw some conclusions in § 9.

2. Experimental model for variations in the supply air temperature

We performed a series of analogue laboratory experiments to model the transient evolution of the flow after a step change in the temperature of the air supply. The experiments were performed in an inverted geometry with dense salt solutions as a proxy for warm air in a real room. Due to the small magnitude of density differences, the flow is Boussinesq, and inverting the geometry will have no significant impact on the dynamics of the experiment.

Obtaining relevant insight from these small-scale experiments relies on achieving geometric and dynamic similarity between the model and the full-scale air flow (Lane-Serff 1989; Savardekar 1990; Lane-Serff, Linden & Smeed 1990; Linden 1999). Achieving geometric similarity is straightforward because most rooms are box-shaped, and the positions of vents and heat sources are easy to match. The relevant dimensionless groups describing the flow dynamics are the Reynolds number, Re, representing the ratio of inertial and viscous forces, and the Péclet number, Pe, representing the ratio of the rate of advection to the rate of diffusion. In the small-scale experiments, the Péclet number refers to salt transport; in the full-scale air flow, the Péclet number refers to heat transport. At both scales, Re and Pe typically have values exceeding 10^3, so the flows are essentially free of viscous and diffusive effects. As a result, the transport of salt or heat is primarily due to turbulent convective fluxes. This experimental technique is well established, and quantitative comparisons between the scales have been used to confirm its accuracy (Lane-Serff 1989; Savardekar 1990).

A Perspex tank, with internal dimensions 0.25 m × 0.25 m × 0.30 m was used to model the interior of a room. This tank was submerged in a larger tank, with dimensions 0.50 m × 0.50 m × 0.65 m, representing the exterior. Fluid was withdrawn from the base of the model room using a peristaltic pump, and holes in the top allowed fluid to flow freely into the model room from the larger tank, modelling a distributed source of ventilation supply air.

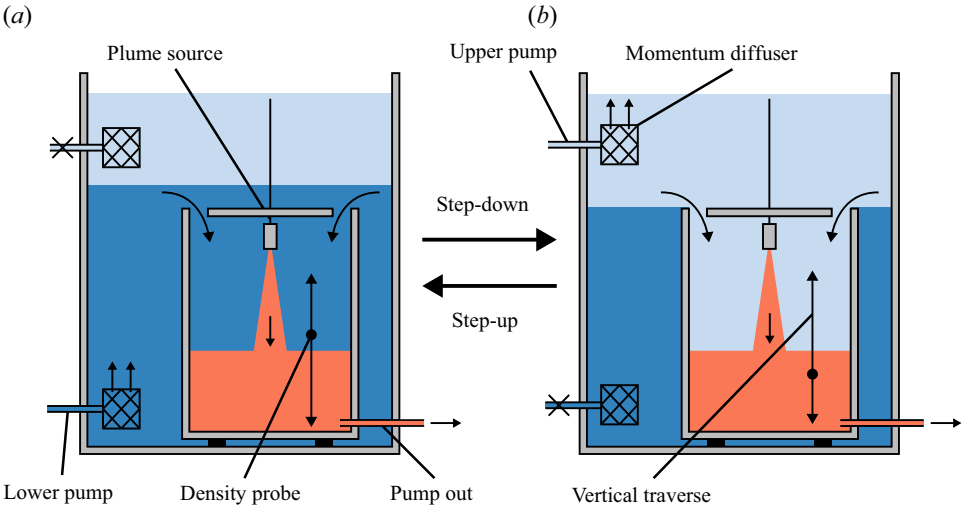

Figure 4. Schematic illustrating the experimental set-up. A small open-topped tank is submerged in a larger tank containing fresh water on top of a layer of salty water. Fluid is withdrawn from the base of the small tank, while the openings in the top allow fluid to flow in from the large tank. The density of the inflow is changed by moving the interface in the outer tank. (*a*) Model of hot inflow , and (*b*) Model of cold inflow

A plume was created by supplying a dense salt solution to a nozzle at the top of the model room, producing a turbulent plume with a relatively small source volume and momentum flux. This nozzle was located at a distance $d \approx 0.1H$ from the top of the model room, where H is the distance from the source to the ceiling of the model room.

By using the pumps to change the height of the density interface in the outer tank, we could switch between a more dense and less dense fluid supply to the model room. We built a two-layer stratification in the outer tank using a pair of peristaltic pumps. The lower pump supplied a dense salty solution, and the upper pump supplied fresh water. Momentum diffusers were added to the inlets to minimise vertical mixing and ensure the density interface was sharp. This apparatus is shown schematically in figure 4.

In a typical experiment, the ventilation and plume pumps were turned on, and the system was run for a sufficiently long time to reach a steady state. Meanwhile, the outer tank was continuously refilled to replace the ventilated fluid. Next, the outer interface was moved so that the density of the inflow changed, and the transient flow began. The experimental conditions are listed in tables 1 and 2, where W_p is the salinity of the plume fluid, πQ_p is the source volume flux, πQ_V is the ventilation volume flux, H is the distance from the plume source to the ceiling, $W_{0,i}$ is the initial salinity of the supply fluid and $W_{0,i}$ is the final salinity of the supply fluid.

In each experiment, the transient evolution was visualised by adding dye to the flow and recording the transient evolution with a DSLR camera (Nikon D3500). In some experiments, the evolution of the vertical density profile was measured using a conductivity probe mounted to a vertical traverse. Fluid is siphoned through the probe to measure conductivity; different salinities change the voltage signal measured by the instrument. This probe is calibrated with a series of standard aqueous solutions of known salinity and density to convert the measured voltage to buoyancy. The disadvantage of this technique is that the probe took approximately 25 s to traverse the height of the tank, which means there is a time difference between the measurements in each profile. However, given that the ventilation time scale was 350−1000 s, each profile gives a reasonable snapshot of the density profile compared with the time scale of ventilation.

W_p (% NaCl)	πQ_p (cm^3 s^{-1})	πQ_V (cm^3 s^{-1})	H (m)	$W_{0,i}$ (% NaCl)	$W_{0,f}$ (% NaCl)	μ	$\hat{g}_0$	Regime
15.0	3.2	35.5	0.31	1.3	0	10.8	−11.0	II
15.0	3.2	35.5	0.31	1.22	0	10.9	−10.2	II
15.0	1.3	25.0	0.26	0.73	0	8.5	−7.8	II
15.0	1.2	29.7	0.20	0.45	0	4.3	−3.2	II
15.0	1.2	35.1	0.20	0.40	0	3.7	−2.8	II
15.0	1.0	26.0	0.26	2.50	0	6.8	−34.8	LI
10.0	1.3	45.6	0.26	1.80	0	3.9	−28.8	LI
15.0	1.2	30.3	0.27	2.00	0	6.8	−25.7	LI
15.0	3.2	70.7	0.31	2.30	0	5.3	−20.6	LI
15.0	3.2	35.5	0.31	2.05	0	10.7	−18.0	LI
15.0	1.2	29.7	0.20	2.23	0	4.1	−17.3	LI
10.0	1.3	45.6	0.27	1.00	0	4.1	−15.0	LI
15.0	1.2	30.3	0.27	1.00	0	6.9	−12.1	LI
15.0	1.2	29.7	0.20	1.55	0	4.2	−11.5	LI
15.0	1.3	45.6	0.26	1.00	0	4.6	−10.9	LI
15.0	1.2	28.8	0.20	1.00	0	4.4	−7.2	LI

Table 1. Experimental conditions for the experiments presented in figure 10 where the buoyancy of the supply fluid was increased.

W_p (% NaCl)	πQ_p (cm^3 s^{-1})	πQ_V (cm^3 s^{-1})	H (m)	$W_{0,i}$ (% NaCl)	$W_{0,f}$ (% NaCl)	μ	$\hat{g}_0$	Regime
7.5	1.2	27.9	0.22	0	0.20	4.4	2.8	LM
7.5	1.2	27.9	0.22	0	0.20	4.4	2.8	LM
15.0	1.3	25	0.26	0	0.73	8.6	7.6	LM
7.5	1.2	27.9	0.22	0	0.75	4.4	9.9	TM
7.5	1.2	27.9	0.22	0	0.75	4.4	9.9	TM
15.0	1.3	45.6	0.26	0	1.00	4.7	10.4	TM
15.0	1.2	30.3	0.27	0	1.00	7.1	11.5	TM
15.0	1.2	30.3	0.27	0	1.00	7.1	11.5	TM
10.0	1.3	45.6	0.27	0	1.00	4.2	13.9	TM
7.5	1.2	27.9	0.22	0	1.15	4.4	15.2	TM
7.5	1.2	27.9	0.22	0	1.30	4.4	17.3	TM
15.0	1.2	30.3	0.27	0	2.00	7.1	23.1	TM
10.0	1.3	45.6	0.26	0	2.40	4.2	33.2	TM

Table 2. Experimental conditions for the experiments presented in figure 10 where the buoyancy of the supply fluid was increased.

3. Experimental observations

Following a step change in the buoyancy of the supply fluid, we identify four new transient flow regimes depending on the magnitude and whether the change involves an increase or decrease of the buoyancy of the supply fluid.

3.1. *Small decrease in the buoyancy of the supply fluid*

Figure 5 shows a series of photographs of an experiment in which there is a small decrease in the buoyancy of the supply fluid. Initially, in panel 1, the system is in steady state, and red dye has been added to the plume to distinguish between the upper

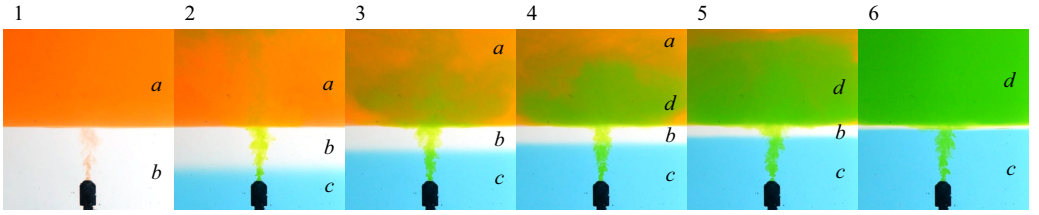

Figure 5. Dye visualisation of an experiment in which there is a small decrease in the buoyancy of the supply fluid. The negatively buoyant supply fluid is dyed blue, and the colour of the dye in the plume is switched from red to green at $t = 0$. The supply fluid fills a new layer (c) below the original stratification (a and b). As the lowest layer (c) deepens, the buoyancy of the plume decreases, and it collapses and intrudes between the original upper and lower layers. The intruding layer (d) grows, replacing the original upper layer (a), which is drained by the ventilation, and the original lower layer (b), which is entrained into the plume. Eventually, the system re-establishes a two-layer stratification (c and d). Panels 1–6 correspond to $t < 0$, $t = 40,\ 120,\ 170,\ 250$ and 580 s, respectively, with $\mu = 4.3$ and $\hat{g}_0 = -3.2$.

layer (a) and the lower layer (b). The new negatively buoyant supply fluid is dyed blue. Additionally, the colour of the plume is switched from red to green once the front of the blue fluid reaches the height of the plume source.

During the experiment, the negatively buoyant supply fluid filled a new layer (c) next to the floor below the original lower layer. As it grows, this new layer (c) contributes an increasing proportion of the total fluid entrained by the plume. As a result, the buoyancy of the plume decreases with respect to the original stratification.

To begin with, in panel 2, the new lowest layer (c) is thin and the plume is positively buoyant in the lower layers (b and c) but is negatively buoyant in the original upper layer (a). Despite this, the plume has enough momentum to reach the ceiling, spread out and mix into the upper layer.

Eventually, in panel 3, the plume entrains enough negatively buoyant fluid from the lowest layer (c) that the negative buoyancy forces acting on the plume in the upper layer (a) cause the plume to stall before reaching the ceiling. In panel 4, the plume has collapsed and become a fountain. Fluid intrudes at the base of the fountain, filling a new green layer (d) between the original layers, and we call this the intermediate intrusion regime. Throughout the transient, the buoyancy of the plume decreases, so the intermediate intrusion is filled from the bottom, producing a stratification within the layer.

Between panels 4 and 6, the original upper layer (a) is extracted by the ventilation and, to a smaller extent, entrained by the fountain. Meanwhile, below the new intrusion (d), the original lower layer (b) is entrained into the plume. Eventually, in panel 6, the system re-establishes a two-layer stratification consisting of the new lower layer (c) and the intruding layer (d). The transient evolution is also shown schematically in figure 2. The shade of blue indicates the buoyancy of the layers.

3.2. *Large decrease in the buoyancy of the supply fluid*

Figure 6 shows a series of photographs of an experiment in which there is a larger decrease in the buoyancy of the supply fluid. Again, we added dye to visualise the flow.

Between panels 1 and 2, the negatively buoyant air supply fills a new layer (c) next to the floor. As we described in § 3.1, the entrainment of fluid from this layer (c) causes the plume to become negatively buoyant with respect to the original upper layer (a) and hence intrudes, filling a new intermediate layer (d).

However, with a large decrease in the buoyancy of the supply fluid, as the lowest layer (c) deepens, the plume becomes negatively buoyant with respect to the original lower layer (b).

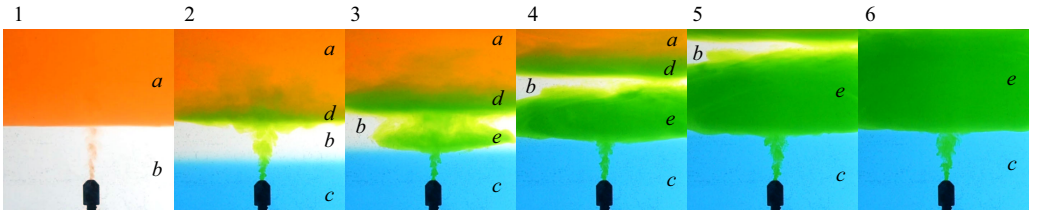

Figure 6. Dye visualisation of an experiment in which there is a large decrease in the buoyancy of the supply fluid. The negatively buoyant supply fluid is dyed blue, and the colour of the dye in the plume is switched from red to green at $t = 0$. The supply fluid fills a new layer (c) below the original stratification (a and b). As the lowest layer (c) deepens, the buoyancy of the plume decreases. This first leads to an intermediate intrusion (d) and then a low-level intrusion (e). The low-level intrusion grows while the higher layers (a, d and b) are successively ventilated, leading to a new two-layer stratification (e and c). Panels 1–6 correspond to $t < 0$, $t = 60,\ 110,\ 210,\ 310$ and 410 s, respectively, with $\mu = 4.1$ and $\hat{g}_0 = -17.3$.

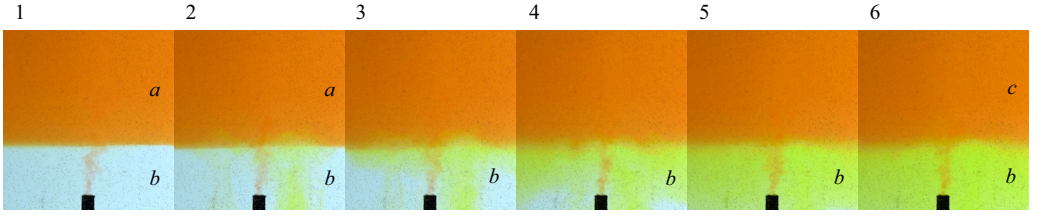

Figure 7. Dye visualisation of an experiment in which there is a small increase in the buoyancy of the supply fluid. The buoyant supply fluid is dyed green and mixed with fluid in the lower layer (b). This mixture is less buoyant than the upper layer (a), so buoyancy forces suppress any mixing, but the changing buoyancy of the plume produces a stratified zone (c) next to the ceiling, which grows to replace the original upper layer that is entrained by the plume. Panels 1–6 correspond to $t < 0$, $t = 15,\ 25,\ 50,\ 75$ and 100 s, respectively, with $\mu = 4.4$ and $\hat{g}_0 = 2.8$.

Eventually, between panels 2 and 3, the negative buoyancy forces acting on the plume are large enough that the plume stalls and forms a fountain within the original lower layer (b). Fluid intrudes at the base of the fountain, filling a new layer (e) below the original lower layer and leaving a band of clear fluid (b) between the two intrusion heights. We call this the low-level intrusion regime. Again, this intruding layer becomes stratified in density because, over time, the buoyancy of the plume gradually decreases as the layer grows.

Between panels 4 and 6, the layers above the intrusion (e) are successively ventilated. First, the original upper layer (a) is ventilated, followed by the intermediate intrusion (d) and, finally, the original lower layer (b), although the fountain may also entrain some of this layer. In panel 6, the system re-establishes a two-layer stratification (e and c). This process is also shown schematically in figure 2, where the shade of blue indicates the average buoyancy of the layers.

3.3. *Small increase in the buoyancy of the supply fluid*

Figure 7 shows a series of photographs of an experiment in which there is a small increase in the buoyancy of the supply fluid. The buoyant supply fluid, which we have dyed green, is gravitationally unstable and mixes with the fluid already in the lower layer (b). This mixture has a mean buoyancy less than the upper layer (a) and, as a result, buoyancy forces suppress any vertical mixing with the upper layer (a). We call this regime lower-layer mixing.

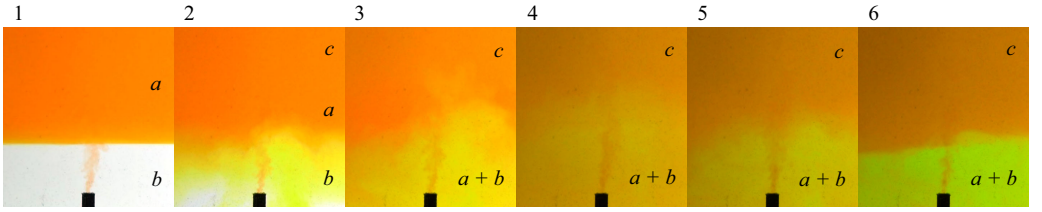

Figure 8. Dye visualisation of an experiment in which there is a large increase in the buoyancy of the supply fluid. The buoyant supply fluid is dyed green and mixed with fluid in the lower layer (b) while the plume stratifies the region next to the ceiling (c). When the buoyancy of the lower layer (b) matches the buoyancy of the original upper layer (a), they overturn. As the buoyancy of the mixing zone (a + b) increases, it erodes the stratified layer (c), which is simultaneously replenished by the plume. Eventually, the buoyancy of the stratified layer (c) exceeds the buoyancy of the supply fluid, and it forms a permanent upper layer, re-establishing a two-layer stratification. Panels 1–6 correspond to $t < 0$, $t = 40$, 110, 650, 830 and 1100 s, respectively, with $\mu = 4.4$ and $\hat{g}_0 = 9.9$.

Across the panels, as time increases, the buoyancy of the lower layer (b) increases, approaching the buoyancy of the supply fluid. The plume entrains this layer, so the buoyancy of the plume fluid also increases in time. As a result, fluid in the plume arriving at the ceiling is the most buoyant fluid in the space, producing a stratified zone (c) next to the ceiling. Since the volume flux supplied by the plume exceeds the ventilation flow, this stratified zone is advected downward by filling-box entrainment (Baines & Turner 1969). This filling front is not distinct because of the particular combination of dyes in figure 7. However, we note that in figure 18, we use a different combination of dyes to observe the descent of this front. It is also shown schematically in figure 3, where the shade of blue indicates the buoyancy of the fluid.

As the stratified zone (c) descends, the plume entrains the original upper layer (a). Eventually, the buoyancy difference between the lower layer (b) and the supply fluid is negligible, so a displacement flow is re-established in the lower layer, and the buoyancy of the plume tends towards a constant value. In the final steady state, the upper layer is homogenised by recirculation through the plume. The buoyancy of both layers has increased, but the buoyancy of the new lower layer is still less than that of the original upper layer.

In addition to the underlying physical processes described above, some non-ideal effects are evident in figure 7. In particular, in the second panel, we see some spatial variation in the fluid supply across the lower layer. As a result, the air supply does not mix uniformly with the fluid already in the lower layer. Rather, natural convection carries it to the top of the lower layer (b), where it overshoots into the upper layer, disturbing the interface and entraining some red dye. The supply fluid is subsequently advected downward through a filling-box-type process, leading to a slight stratification in the lower layer. However, the turbulent mixing through the lower layer is relatively fast, so in the models later in the paper, we assume that the buoyancy of the lower layer is uniform and gradually increases in time.

3.4. *Large increase in the buoyancy of the supply fluid*

Figure 8 shows photographs of an experiment in which the supply fluid has a large increase in buoyancy. In panel 1, the system is in steady state; red dye is added to the plume, allowing us to distinguish the red upper layer (a) from the clear lower layer (b). Green dye was added to the buoyant supply fluid to visualise the transient evolution of the flow as the buoyancy of the supply fluid is increased.

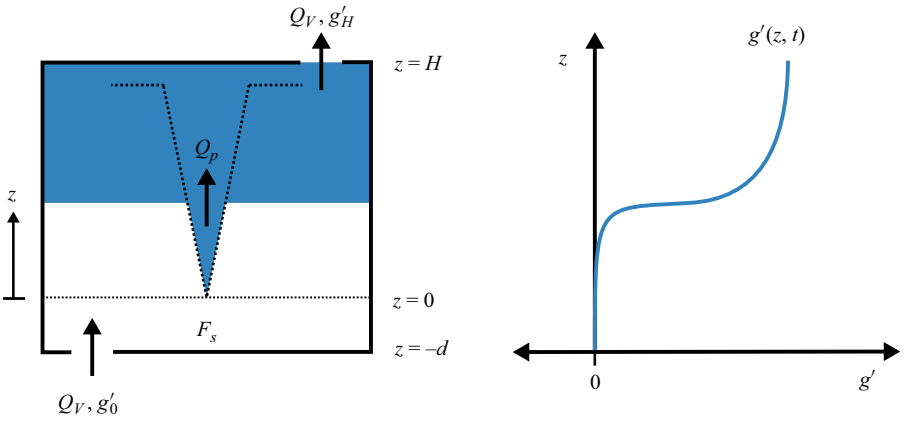

Figure 9. Schematic of displacement ventilation.

The early evolution of the flow is identical to the small-increase case (see figure 7). In panel 2 of figure 8, the supply fluid mixes into the lower layer (b), and the mixture is less buoyant than the original upper layer (a); this largely confines the mixing to the original lower layer (b). As before, the buoyancy of the lower layer (b) increases and, in turn, increases the buoyancy of the plume, so a stratified zone (c) develops next to the ceiling.

However, with a sufficiently large increase in the buoyancy of the supply fluid, the buoyancy of the lower layer (b) eventually increases so as to match the buoyancy of the original upper layer (a). As a result, between panels 2 and 3, the evolving lower layer (b) and the original upper layer (a) overturn, producing a combined mixing zone ($a + b$) and transporting red dye downward. We call this the total mixing regime. Immediately after overturning, the mixing zone ($a + b$) extends from the floor to the bottom of the stratified zone (c), where, again, buoyancy forces suppress the expansion of the mixing zone.

Across the remaining panels, the buoyancy of the mixing zone ($a + b$) increases towards the buoyancy of the supply fluid, allowing it to erode the stratified layer (c). This leads to a dynamic equilibrium between replenishment of the stratified layer (c) by the plume and erosion into the mixed zone ($a + b$).

A significant change occurs between panels 4 and 5 when the buoyancy of the plume fluid reaching the ceiling exceeds the buoyancy of the ventilation supply fluid for the first time. Fluid above this first front cannot be eroded into the mixing zone ($a + b$) and instead a filling front descends, forming a new permanent upper layer. Later, in panel 6, the plume has entrained the red dye from the lower layer and re-established a two-layer stratification (c and $a + b$). In the final steady state, the buoyancies of both layers are greater than that of the original upper layer. This process is also shown schematically in figure 3, where the shade of blue indicates the buoyancy of the layers and in figure 20 which shows a composite image of the transient.

4. Theoretical development

To model the system, we draw on the model of a turbulent plume rising from a constant source of buoyancy, πF_s, in a room of total height $H + d$ and uniform cross-sectional area πA. We let z denote the vertical distance above the source, where the upper and lower vents are located at $z = H$ and $z = -d$, respectively. The ventilation volume flux πQ_V is constant, and the supply air has buoyancy $g'_0(t)$, this generating a stratification $g'(z, t)$ in the room (figure 9).

At this point, it is important to note that in our experiments, the plume source has a finite height, d, above the floor, which has some implications for the evolution of the flow. On the one hand, when the buoyancy of the supply fluid decreases, this extra depth introduces a time delay, $t_d = Ad/Q_V$, before the change in the supply fluid impacts the plume and changes the flow. On the other hand, when the buoyancy of the supply fluid increases, the extra depth adds to the inertia of the system, delaying the time before overturn because the system is mixing a larger volume of fluid. As a result, it is important to account for this extra depth when we model the evolution of the stratification in §§ 6 and 7

4.1. *Plume theory*

A turbulent plume rising from a localised source of buoyancy in a quiescent environment can be modelled in terms of the fluxes of volume πQ (dimensions $\mathrm{L}^3\ \mathrm{T}^{-1}$, where L is length and T is time), momentum πM ($\mathrm{L}^4\ \mathrm{T}^{-2}$) and buoyancy πF ($\mathrm{L}^4\ \mathrm{T}^{-3}$). For a Boussinesq plume, the conservation equations are

$$\frac{\mathrm{d}Q}{\mathrm{d}z} = 2\alpha M^{1/2}, \quad \frac{\mathrm{d}M}{\mathrm{d}z} = \frac{FQ}{M}, \quad \frac{\mathrm{d}F}{\mathrm{d}z} = -N^2 Q, \tag{4.1}$$

where $\alpha \approx 0.13$ is the entrainment coefficient appropriate for top-hat profiles (Morton *et al.* 1956), z is the vertical coordinate measured from the source and, if the ambient stratification is continuous, it is given by the Brunt–Väisälä frequency,

$$N^2 = -\frac{g}{\rho_r}\frac{\mathrm{d}\rho_e}{\mathrm{d}z} = \frac{\mathrm{d}g'}{\mathrm{d}z}, \tag{4.2}$$

where $\rho_e(z)$ is the fluid density outside the plume. These equations are derived for unconfined plumes but can also be used for confined plumes as long as the cross-sectional area of the plume is much less than that of the enclosure (Baines & Turner 1969).

In general, the source conditions are $Q = Q_s$, $M = M_s$ and $F = F_s$ at $z = 0$, and the plume equations need to be solved numerically. However, in a uniform environment ($N^2 = 0$), the buoyancy flux in the plume is conserved, and there is a similarity solution for a pure source of buoyancy ($Q_s = M_s = 0$, $F_s \neq 0$), where

$$Q(z) = \left(\frac{6\alpha}{5}\right)\left(\frac{9\alpha}{10}\right)^{1/3} F_s^{1/3} z^{5/3}, \quad M(z) = \left(\frac{9\alpha}{10}\right)^{2/3} F_s^{2/3} z^{4/3}, \quad F = F_s. \tag{4.3}$$

If the environment is stably stratified ($N^2 > 0$), the buoyancy flux in a plume decreases with height and will fall to zero at the neutral buoyancy height, z_n. Above this height, buoyancy forces oppose the fluid motion, causing the plume to reach a maximum height, z_m, at which the momentum flux equals zero. The flow reverses direction and falls back down around the rising core, forming a fountain. Inside this fountain, the interaction between the rising and falling flows substantially changes the dynamics, and the fountain settles at a steady height, z_{ss}, lower than the initial maximum, z_m. Eventually, fluid in the descending annular plume spreads out to form an intrusion close to the neutral height, z_n.

The ranges of dynamics exhibited by fountains in various environments are discussed in detail elsewhere (see e.g. Hunt & Burridge 2015). However, in principle, the plume equations can be extended to model a fountain by making additional entrainment hypotheses to describe the entrainment of ambient fluid into the fountain and between the rising core and falling annulus (Mcdougall 1981; Bloomfield & Kerr 2000). Unfortunately, this requires the calculation of both the rising and falling flows and the introduction of several free parameters into the model. Therefore, building on past experimental and theoretical results (e.g. Kumagai 1984; Baines, Turner & Campbell 1990; Lin & Linden

2005*b*; Bower *et al.* 2008; Lima Neto *et al.* 2016), we use a simplified model for penetrative entrainment by a negatively buoyant fountain without an explicit characterisation of the flow.

Dimensional arguments suggest that the total volume flux entrained by the fountain scales with the volume flux in the plume at the neutral level (Kumagai 1984; Bower *et al.* 2008). Thus,

$$Q_e = EQ(z_n), \tag{4.4}$$

where $E = E(Fr)$ is the penetrative entrainment rate that generally depends on the local Froude number:

$$Fr = \frac{M^{5/4}}{Q|F|^{1/2}}. \tag{4.5}$$

Kumagai (1984) developed an empirical correlation for penetrative entrainment across a density interface, where

$$E = \frac{Fr}{1 + 3.1Fr^3 + 1.8Fr^3}. \tag{4.6}$$

Entrainment decreases with decreasing Fr, and if $Fr \ll 1$, then entrainment of ambient fluid into the fountain is negligible, $E \approx 0$, and all of the fluid overshooting the neutral level intrudes around the neutral height without changing density or concentration.

4.2. *Non-dimensionalisation*

We introduce scalings based on a hypothetical pure plume rising through a uniform layer of reference fluid to a height $z = H$. Using (4.3), the volume, momentum and buoyancy fluxes in this reference plume are $Q_r(H)$, $M_r(H)$ and F_s, respectively. These definitions lead to the dimensionless variables

$$\xi = \frac{z}{H}, \quad q = \frac{Q}{Q_r(H)}, \quad m = \frac{M}{M_r(H)}, \quad f = \frac{F}{F_s} \quad \text{and} \quad \hat{g} = \frac{g' Q_r(H)}{F_s}. \tag{4.7}$$

With these definitions, (4.1) become

$$\frac{\mathrm{d}q}{\mathrm{d}\xi} = \frac{5}{3} m^{1/2}, \quad \frac{\mathrm{d}m}{\mathrm{d}\xi} = \frac{4}{3}\frac{fq}{m}, \quad \frac{\mathrm{d}f}{\mathrm{d}\xi} = \frac{\mathrm{d}\hat{g}}{\mathrm{d}\xi} q, \tag{4.8}$$

and the Froude number is

$$Fr = \left(\frac{5}{8\alpha}\right)^{1/2} \frac{m^{5/4}}{q|f|^{1/2}}. \tag{4.9}$$

Finally, we scale time with the filling-box time, which is defined as

$$T_f = \frac{AH}{Q_r(H)}. \tag{4.10}$$

This is the time required to fill a room with volume πAH with the volume flux $\pi Q_r(H)$. The dimensionless time is then

$$\tau = \frac{t}{T_f}. \tag{4.11}$$

5. Predicting the flow regime

In § 2, we described the four transient flow regimes: low-level intrusion, intermediate intrusion, low-level mixing and total mixing. We now develop simple criteria to predict the flow regime following a step change in the buoyancy of the supply air.

5.1. *Intermediate intrusion regime*

When the buoyancy of the supply fluid decreases, it fills a new cold layer below the original stratification. Following this decrease in the buoyancy of the supply fluid, the plume will always become negatively buoyant with respect to the original upper layer, and the criterion for an intermediate intrusion is

$$\hat{g}_0 < 0. \tag{5.1}$$

5.2. *Low-level intrusion regime*

As the lowest layer grows, the plume will become negatively buoyant with respect to the original lower layer, leading to a low-level intrusion if

$$1 + \hat{g}_0 \xi_1^{5/3} < 0 \tag{5.2}$$

for some value of ξ_1, the interface height between the new lowest layer and the original lower layer. The height of this interface increases until it reaches the steady-state interface depth ($\xi = \mu^{-3/5}$; (1.2)). Therefore, the condition for a low-level intrusion can be written as

$$\hat{g}_0 < -\mu_0. \tag{5.3}$$

5.3. *Low-level mixing regime*

When the buoyancy of the supply fluid increases, it will spontaneously mix with fluid in the lower layer. Therefore, lower-layer mixing occurs when

$$\hat{g}_0 > 0. \tag{5.4}$$

5.4. *Total mixing regime*

In the case that the buoyancy of the supply fluid increases, the original upper layer will overturn once the buoyancy of the evolving lower layer matches the buoyancy of the original upper layer. To reach this condition, the buoyancy of the supply fluid should be greater than that of the original upper layer. Non-dimensionalisation of (1.5) leads to the condition

$$\hat{g}_0 > \mu_0. \tag{5.5}$$

5.5. *Regime diagram*

The criteria described above categorise the transient evolution into the four regimes based on the buoyancy change $\hat{g}_0$ and the degree of ventilation, described by the parameter μ. In figure 10, these have been plotted together with experimental observations in a regime diagram. The predicted regimes are consistent with the experimental observations of under-ventilated systems in the range $3 \lesssim \mu \lesssim 12$. However, we are limited by the number of experimental observations close to regime transitions where the system can exhibit some resistance to change. The grey-shaded region indicates the over-ventilated regime ($\mu < 2$) in which the ventilation flow is very large and approaches or exceeds the flow in the plume. In over-ventilated systems, the idealised volume balance model is not applicable

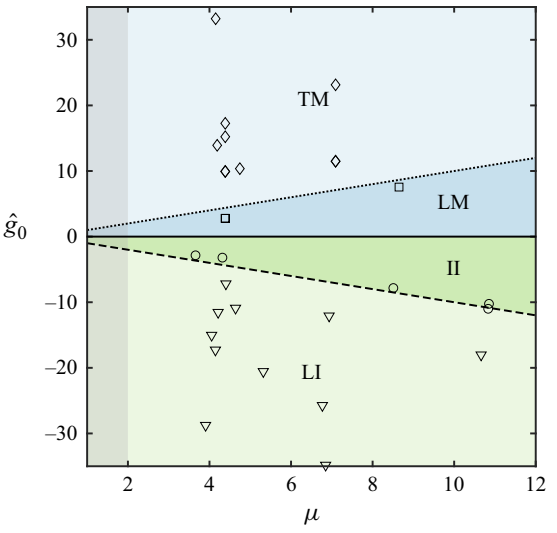

Figure 10. Regime diagram for the transient flows following a step change in the temperature of the air supply in terms of the size of the temperature change, $\hat{g}_0$, and the degree of ventilation, μ. The solid horizontal line represents no change from the initial steady state, the dashed line separates intermediate intrusions (II, small decrease in buoyancy) and low-level intrusions (LI, large decrease in buoyancy) and the dotted line separates lower-layer mixing (LM, small increase in buoyancy) and total mixing (TM, large increase in buoyancy). The symbols correspond to experiments where intermediate intrusions (○), low-level intrusions (▽), lower-layer mixing (□) or total mixing (◇) were observed.

(Toy & Woods 2024), but approximate criteria may still provide useful insight into the expected flow.

As a note of caution, we highlight that (5.1) and (5.2) were developed based on the buoyancy flux of the plume. In an unconfined environment, a negatively buoyant plume will always intrude. However, in a confined space, if the plume has enough momentum, the negative buoyancy forces may be unable to arrest the plume before it hits the ceiling. This can lead to mixing throughout the upper layer rather than forming an intrusion. The impact of momentum flux on the regime boundaries is explored in Appendix A.

6. Models for the transient flow after decreasing the buoyancy of the supply fluid

In §§ 3.1 and 3.2, we described how decreasing the buoyancy of the supply fluid changed the flow. We now develop models to describe the evolution of the layer depths and buoyancy as a function of time.

For simplicity, we neglect the internal stratification within each layer and assume that the buoyancy profile can be approximated as a staircase of well-mixed layers separated by sharp interfaces. Furthermore, we assume that the plume evolves over a much shorter time scale than the surrounding stratification. Therefore, the plume equations can be integrated numerically between the finite source and the ceiling during each time step, assuming the surrounding stratification is steady. At each layer interface, we assume that the volume and momentum fluxes in the plume are continuous but account for the discrete change to the plume buoyancy flux, f, caused by the difference in the buoyancy, $\hat{g}$, of the layers.

6.1. *Pre-intrusion*

When the buoyancy of the supply fluid decreases, it fills a new negatively buoyant layer which will eventually cause the plume to intrude between the original upper and lower

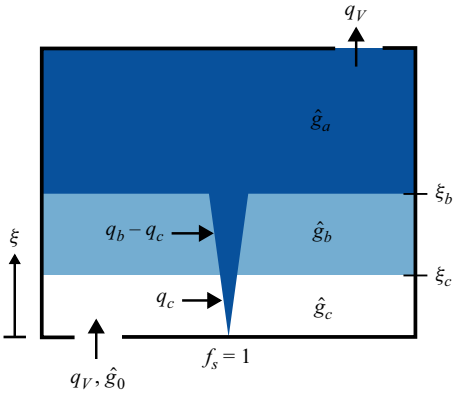

Figure 11. Schematic of the pre-intrusion regime, illustrating the dimensionless variables used.

layers. However, initially the plume has enough momentum to reach the ceiling, spread out and mix throughout the upper layer. As a limiting condition for the models, we assume that an intrusion will form once the momentum flux in the plume falls to zero at the ceiling ($m = 0$ at $\xi = 1$).

From the start of the experiment until the onset of the intrusion, we model the stratification as three well-mixed layers. As before, we label each layer (a–c) sequentially according to the age of the fluid. Interface ξ_i is at the top of layer i and the volume flux in the plume is q_i at this height. This notation and the fluxes into and out of each layer are shown schematically in figure 11. Performing mass balances leads to equations for the interface evolution:

$$\frac{\mathrm{d}\xi_c}{\mathrm{d}\tau} = q_V - q_c \quad \text{and} \quad \frac{\mathrm{d}\xi_b}{\mathrm{d}\tau} = q_V - q_b, \tag{6.1}$$

where $q_V = 1/\mu$ is the ventilation volume flux. The buoyancy of the original lower layer, $\hat{g}_b$, and the new lowest layer, $\hat{g}_c$, are constant, but the buoyancy of the original upper layer, $\hat{g}_a$, evolves in time. Conservation of the total buoyancy within the upper layer leads to

$$\frac{d\big(\hat{g}_a(1-\xi_b)\big)}{\mathrm{d}\tau} = 1 + \hat{g}_c q_c + \hat{g}_b\,(q_b - q_c) - \hat{g}_a q_v, \tag{6.2}$$

where the terms on the right-hand side correspond to the buoyancy flux from the plume source, buoyancy entrained from the new lowest layer (c) and original lower layer (b) and buoyancy extracted by the ventilation, respectively. These equations can be solved using initial conditions based on the starting steady state. For an under-ventilated system, these are $\xi_c = 0$, $\xi_b = \mu^{-3/5}$, $\hat{g}_c = \hat{g}_0$, $\hat{g}_b = 0$ and $\hat{g}_a = \mu$.

6.2. *Intermediate intrusion*

Once the buoyancy forces are just able to arrest the plume at $\xi = 1$, we assume that the plume collapses and intrudes. Introducing a new layer (d) below the original upper layer (a), the evolved system has four layers separated by three interfaces. The fluxes into and out of each layer are shown schematically in figure 12. Compared with the previous three-layer model, there is one new category of flux, Eq_d, to model penetrative entrainment by the fountain (see § 4.1). Performing a mass balance over each of the layers, the new equations for the interface evolution are

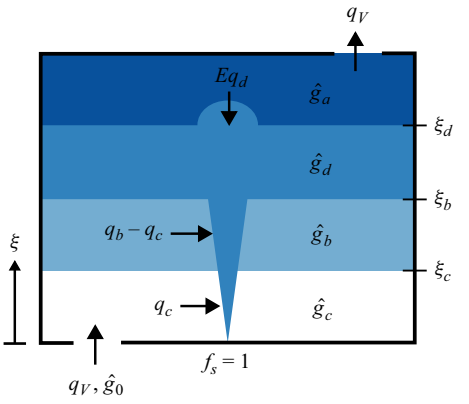

Figure 12. Schematic of the intermediate intrusion regime, illustrating the dimensionless variables used.

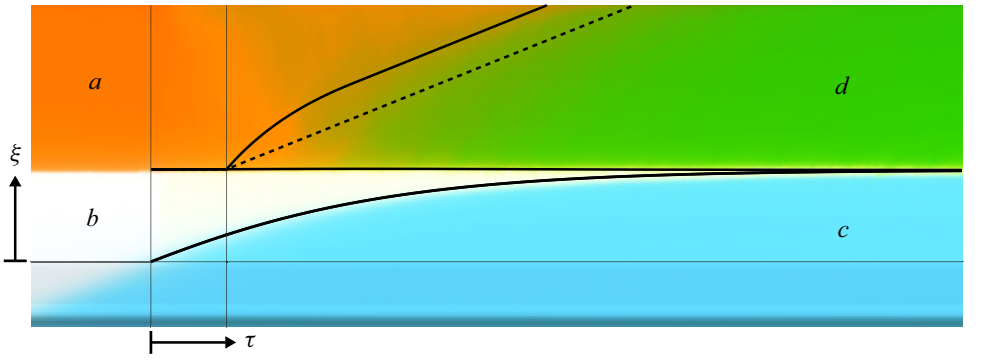

Figure 13. Composite image showing the horizontally averaged pixel intensity during an intermediate intrusion where $\mu = 4.3$ and $\hat{g}_0 = -3.2$ for $\tau < 7$. The image has been annotated with the predicted interface depths using the well-mixed model. The thick black lines correspond to the interface heights in the full model, while the dashed line shows the model prediction for the top of the intruding layer (d) without penetrative entrainment. The horizontal line indicates the height of the source, and the vertical lines indicate the start of the transient and when the plume momentum is equal to zero at the ceiling.

$$\frac{\mathrm{d}\xi_c}{\mathrm{d}\tau} = q_V - q_c, \quad \frac{\mathrm{d}\xi_b}{\mathrm{d}\tau} = q_V - q_b, \quad \frac{\mathrm{d}\xi_d}{\mathrm{d}\tau} = q_V + Eq_d, \tag{6.3}$$

and the total buoyancy of the intruding layer (d) evolves according to

$$\frac{d\left(\hat{g}_d(\xi_d - \xi_b)\right)}{\mathrm{d}\tau} = 1 + \hat{g}_c q_c + \hat{g}_b\,(q_b - q_c) + \hat{g}_a E q_d. \tag{6.4}$$

The terms on the right-hand side correspond to the buoyancy flux from the plume, entrainment from the layers below the intrusion and penetrative entrainment from the layer above the intrusion, which all have constant buoyancies.

In figure 13, we use this well-mixed model to predict the interface heights and superpose these predictions onto a composite image showing the horizontally averaged pixel intensity at each height (y axis) as a function of time (x axis) during an experiment in which an intermediate intrusion formed, where $\mu = 4.3$ and $\hat{g}_0 = -3.2$. The thin horizontal line indicates the height of the plume source, and $t = 0$, which corresponds to the time when the blue fluid front reaches the plume source, is shown by the first vertical line.

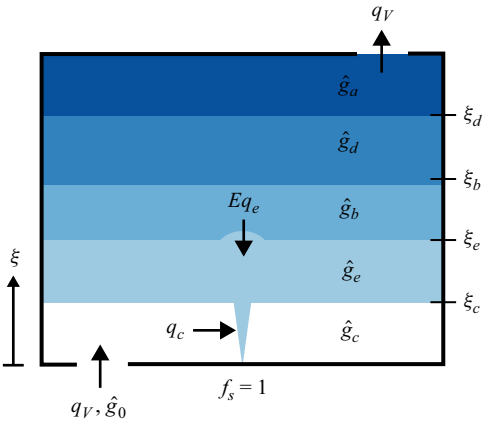

Figure 14. Schematic for the low-level intrusion regime, illustrating the dimensionless variables used.

Overall, the well-mixed model describes the main features of the transient evolution reasonably well. In particular, it replicates experimental observations of the growth of the new lowest layer (c) and entrainment of the original lower layer (b). Furthermore, using the momentum condition to switch between the three- and four-layer models (second vertical line) agrees well with the time when green fluid starts to descend.

The model assumes that the intruding layer (d) forms immediately after the momentum in the plume is equal to zero at the ceiling. However, in the experiments, there is a significant time scale over which fluid descends to fill the intruding layer (d). For comparison, we present the predicted interface depth with (solid line) and without (dashed line) penetrative entrainment. Overall, the model with penetrative entrainment is a significantly better match with the experiments. In particular, it provides a more accurate prediction of when the original upper layer (a) is fully ventilated. However, there is some significant uncertainty because of the diffuse boundary between the layers rather than the sharp interface assumed in the modelling.

Comparing the models with (solid) and without (dashed) penetrative entrainment, we see that including the effect of penetrative entrainment causes the intruding layer (d) to grow at a much faster rate initially. However, this speed decreases in time, eventually matching the model without penetrative entrainment. This is because, initially, the fountain is very strong (large Fr) and entrains a significant volume of fluid from the upper layer. However, it becomes weaker throughout the transient. Eventually, the fountain does not exit the intruding layer, and the penetrative entrainment ceases. As a result, the flux due to penetrative entrainment is only significant at early times, but this leads to a permanent offset in the position of the interface.

6.3. *Low-level intrusion*

If the buoyancy decrease is sufficient then eventually the plume can become dense in the original lower layer (b). At this time, we introduce a new layer (e), leading to a five-layer model for the flow, where the initial conditions for this model are the final conditions from the four-layer model. The fluxes into and out of each layer are shown in figure 14. Performing mass balances on each layer leads to

$$\frac{\mathrm{d}\xi_c}{\mathrm{d}\tau} = q_V - q_c, \quad \frac{\mathrm{d}\xi_e}{\mathrm{d}\tau} = q_V + Eq_e, \quad \frac{\mathrm{d}\xi_b}{\mathrm{d}\tau} = \frac{\mathrm{d}\xi_d}{\mathrm{d}\tau} = q_V, \tag{6.5}$$

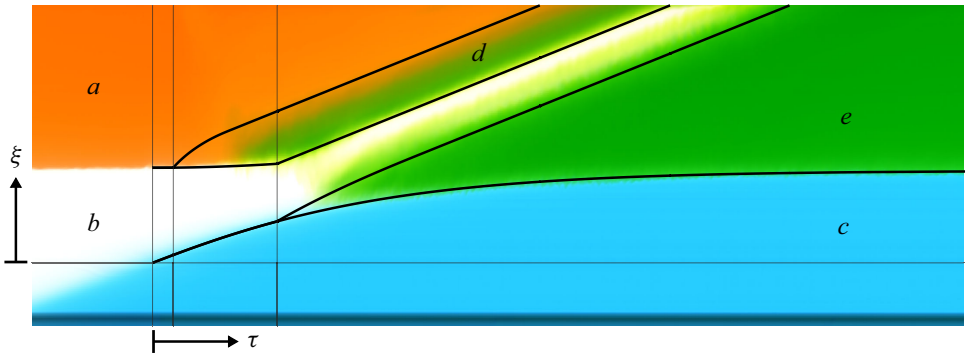

Figure 15. Composite image showing the horizontally averaged pixel intensity during an intermediate intrusion where $\mu = 4.1$ and $\hat{g}_0 = -17.3$ for $\tau < 7$. The image has been annotated with the predicted interface depths using the well-mixed model. The dashed line shows the model prediction without penetrative entrainment. The horizontal line indicates the height of the source, and the vertical lines indicate the start of the transient and when the plume momentum is equal to zero at the ceiling.

and the total buoyancy of the new intruding layer (e) evolves according to

$$\frac{\mathrm{d}\left(\hat{g}_e\,(\xi_e - \xi_c)\right)}{\mathrm{d}\tau} = 1 + \hat{g}_c q_c + \hat{g}_b E q_e, \tag{6.6}$$

with all other layers having a constant buoyancy.

In figure 15, we use the series of models to predict the interface heights and superpose these predictions onto a composite image showing the horizontally averaged pixel intensity at each height (y axis) as a function of time (x axis) during an experiment in which a low-level intrusion was formed. In this case, $\mu = 4.1$ and $\hat{g}_0 = -17.3$.

We see that the time predicted by the model for the onset of the low-level intrusion (third vertical line) agrees well with the descent of green fluid through the original lower layer (b). However, it appears that the model systematically under-predicts the height of the intruding layer (e). Comparing the composite image with the photographs in figure 6, we see that the intruding layer has a finite depth as it starts to intrude and a curved upper surface, which persists during the transient and is advected upwards. This is propagated through the averaging process and causes the gradient at the top of the intrusion which is not captured by the model. Below this gradient zone the layer is close to uniform and the growth of this uniform layer is consistent with the model.

In figure 16, we compare the buoyancy profile predicted by the well-mixed models (green) with that measured using the conductivity probe (blue) during an experiment where $\mu = 4.6$ and $\hat{g}_0 = -10.9$ and a low-level intrusion was formed. The experimental profile is continuously stratified, as we might expect because the buoyancy of the plume continuously decreases in time. However, despite the simplifying assumption of well-mixed layers, the agreement between the model and experiment is reasonable.

7. Models for the transient flow after increasing the buoyancy of the supply fluid

In §§ 3.3 and 3.4, we described how increasing the buoyancy of the supply fluid led to mixing between the supply fluid and the fluid already in the space and how the extent of mixing depends on the magnitude of the buoyancy increase. If the decrease was small, the mixing zone was confined to the original lower layer, whereas, for large increases, the original upper layer was also overturned.

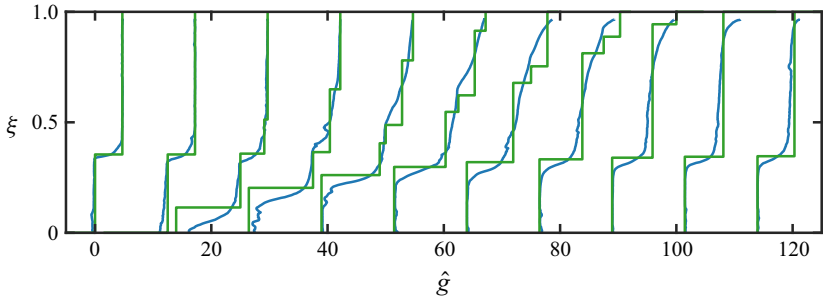

Figure 16. Evolution of the buoyancy profile outside the plume during a low-level intrusion in which $\mu_0 = 4.6$ and $\hat{g}_0 = -10.9$. Profiles are shown for $0 < \tau < 6$ with $\Delta\tau = 0.6$. Each profile has been offset by a distance proportional to the time of the measurement.

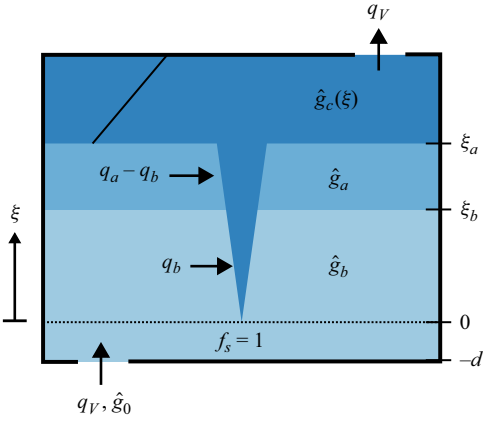

Figure 17. Schematic for low-level mixing, illustrating the dimensionless variables used.

For simplicity, we model the case of a uniformly distributed air supply with no horizontal variation in the mixing. We do, however, account for any extra depth, d, below the heat source as discussed in § 4. This extra volume may be a large proportion of the volume of the lower layer and has a significant impact on the evolution of buoyancy.

7.1. *Lower-layer mixing regime*

During lower-layer mixing, there is little disturbance to the original interface between the upper and lower layers. However, as the lower layer becomes progressively more buoyant, so does the fluid in the plume at the top of the space. As a result, a stratified front of fluid supplied by the plume descends from the ceiling. Labelling each layer (a–c) sequentially according to the age of the fluid, we assume the two lower layers are well mixed while the third is not. This is shown schematically in figure 17. Performing mass balances over the lower two layers leads to equations for the interface evolution:

$$\frac{\mathrm{d}\xi_b}{\mathrm{d}\tau} = q_V - q_b, \quad \frac{\mathrm{d}\xi_a}{\mathrm{d}\tau} = q_V - q_a. \tag{7.1}$$

Furthermore, conservation of the total buoyancy in the lower layer leads to

$$\frac{d\big(\hat{g}_b(\xi_b + d)\big)}{\mathrm{d}\tau} = \hat{g}_0 q_V - \hat{g}_b q_b. \tag{7.2}$$

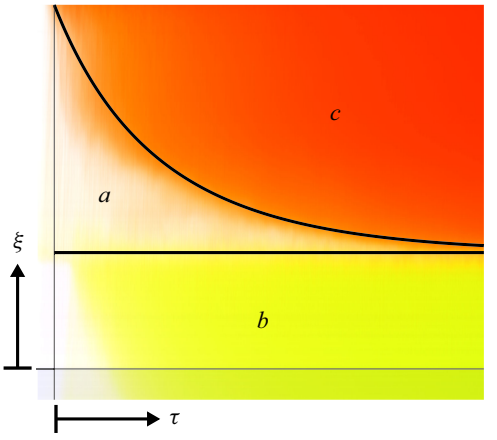

Figure 18. Composite image showing the horizontally averaged pixel intensity during lower-layer mixing where $\mu = 4.4$ and $\hat{g}_0 = 2.8$ for $\tau < 3.6$. The image has been annotated with the predicted interface depths using the well-mixed model. The horizontal line indicates the height of the source, and the vertical line indicate the start of the transient.

The buoyancy of the original upper layer, $\hat{g}_a$, is constant, and, for now, we will not explicitly model the stratified layer, $\hat{g}_c(\xi)$ (see § 7.2). For under-ventilated systems, the appropriate initial conditions are $\xi_b = \mu^{-3/5}$, $\xi_a = 1$, $\hat{g}_b = 0$ and $\hat{g}_a = \mu$,

In figure 18, we use this well-mixed model to predict the interface heights and superpose these predictions onto a composite image showing the horizontally averaged pixel concentration at each height (y axis) as a function of time (x axis). To observe the descent of the stratified front, we show an experiment in which the starting steady state is reached without dye. Then, at $t = 0$, when we increase the buoyancy of the supply fluid we add green dye to the supply fluid and red dye to the plume. During the transient, there is no noticeable change in the depth of the interface between the lower layer and the original upper layer. However, the fluid mixing into the lower layer does overshoot the interface, which may lead to penetrative entrainment.

The predicted depth of the first front is in accord with the motion of the dye front. However, it appears that the impact between the plume and the ceiling leads to an additional mixing process, accelerating the fluid's downward transport at early times. This mixing is less pronounced at later times because entrainment into the plume makes the interface sharper.

7.2. *Total mixing regime*

In § 3.4, we described how the stratified layer at the top of the room is continuously eroded by the mixed region and replenished by the plume. As a result, assuming that each layer is well mixed is insufficient to describe the transient flow. However, the model for the lower-layer mixing regime can also be applied to larger buoyancy increases to predict the time, τ_0, when the original upper and lower layers overturn.

Assuming that the depth of the lower layer is constant and is equal to the steady-state interface depth (1.2), then $q_b = q_V = 1/\mu$, and (7.2) can be solved, leading to

$$\tau_o = \left(\mu^{-3/5} + d\right)\mu \ln\left(\frac{\hat{g}_0}{\hat{g}_0 + \mu}\right). \tag{7.3}$$

To model the full system evolution, the ambient stratification is discretised into a large number of uniform layers, and at each time step, the plume equations are solved. The

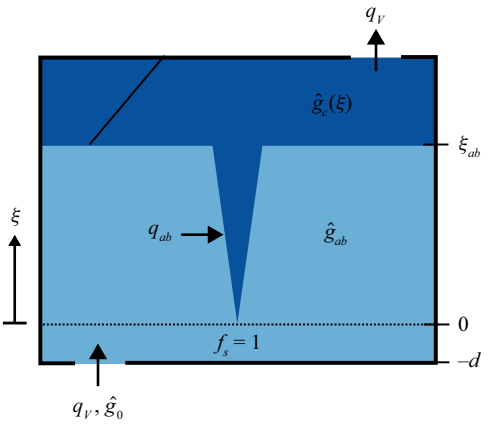

Figure 19. Schematic for total mixing, illustrating the dimensionless variables used.

interfaces are then advected with a velocity

$$\hat{v}_i = q_v - q_i, \tag{7.4}$$

so that their new position is given by

$$\xi_i(\tau + \Delta\tau) = \xi_i(\tau) + \hat{v}_i \Delta\tau. \tag{7.5}$$

The advection of the interface captures the process of entrainment by the plumes so that the layer depth will decrease at the end of every time step. A new layer, with the same buoyancy as the plume, is added to account for fluid transported to the ceiling by the plume. Furthermore, a second new layer is added next to the floor to account for the fluid supplied by the ventilation.

When buoyant fluid is supplied next to the floor, the stratification becomes unstable. We assume that this leads to a rapid process of vertical mixing until the stratification stabilises. This process is modelled by iteratively merging the unstable layer with the layer above until the average buoyancy of the merged layer is less than that of the next layer. This occurs when

$$\hat{g}_{n+1} > \frac{\sum_{i=1}^{n} (\xi_i - \xi_{i-1})\, \hat{g}_i}{\xi_n - \xi_0}, \tag{7.6}$$

where $\xi_0 = -d$.

In figure 20, we show the predictions of this model for the height of the lower mixed layer (solid), the evolution of the first stratified front (dotted) and the evolution of the first permanent front (dashed). These are superposed on a composite image showing the horizontally averaged pixel intensity at each height (y axis) as a function of time (x axis). We have also labelled each region in accord with the qualitative descriptions provided in § 3.4.

We see that the model captures the key features of the flow. However, the impact of non-uniform supply is significantly greater, with a larger increase in the buoyancy of the source fluid, leading to localised upward flows and some mixing between the lower and upper layers.

Figure 21 compares the buoyancy profile predicted by the stratified model (green) and the measured buoyancy profile from the conductivity probe (blue) during an experiment where $\mu_0 = 4.7$ and $\hat{g}_0 = 10.4$. There is reasonable agreement between the model and the experimental measurements in the upper part of the room and at late times. However, there

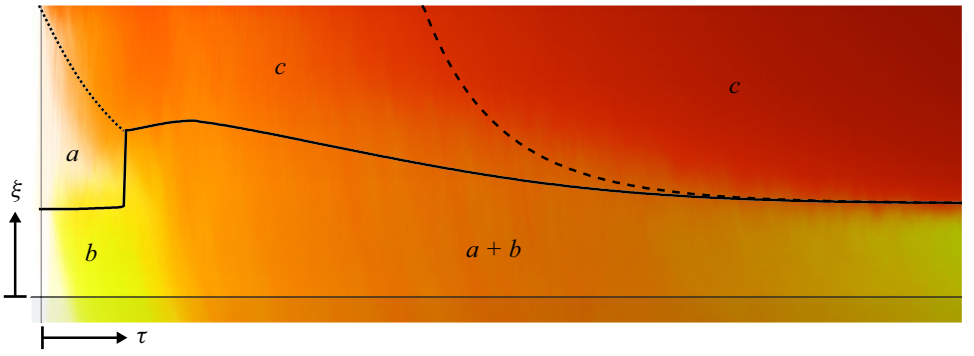

Figure 20. Composite image showing the horizontally averaged pixel intensity during total mixing where $\mu = 4.4$ and $\hat{g}_0 = 9.9$ for $\tau < 10$. The image has been annotated with the predictions from the stratified model. The dotted line shows the descent of the stratified zone (c), the dashed line shows the descent of the first permanent front of fluid and the thick solid line shows the predicted extent of the mixing zone. The horizontal line indicates the height of the source, and the vertical lines indicate the start of the transient.

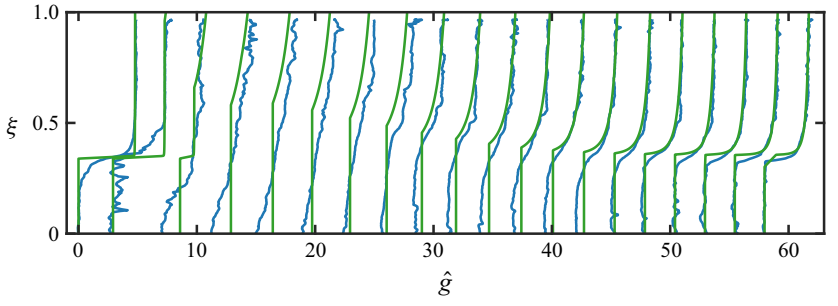

Figure 21. Evolution of the buoyancy profile outside the plume during total mixing in which $\mu_0 = 4.7$ and $\hat{g}_0 = 10.4$. Profiles are shown for $0 < \tau < 11.4$ with $\Delta\tau = 0.6$. In each experiment the profile has been offset in the positive x direction by a distance proportional to the time of the measurement.

is less agreement in the lower part of the space at early times. In part, this difference arises because, in the experiment, the buoyant air supply at the base of the room is not uniformly distributed across the space. Instead, the localised regions of supply lead to some buoyancy instability and localised zones of flow. As a result, the evolution of the lower layer follows a filling-box-type flow process where the supply fluid rises to the top of the layer entraining fluid and this leads to mixing of the fluid below (cf. Baines & Turner 1969).

8. Discussion

In some buildings, the control system may change the temperature of the supply air depending on the time, the expected occupancy or the external conditions, and this may lead to a transient adjustment of the overall ventilation flow. In the previous section, we developed models for each of the four transient flow regimes and demonstrated that these are consistent with our experimental observations. We now use these models to predict the time scale over which the system adjusts from one steady state to the next to assess the fraction of time during which we might expect to observe transient ventilation flows and the significance of this for the comfort and health of the occupants.

Figure 22 shows the adjustment time scale as a function of the buoyancy change for three model systems where $\mu = 2$, 4 and 8, corresponding to steady-state interface depths

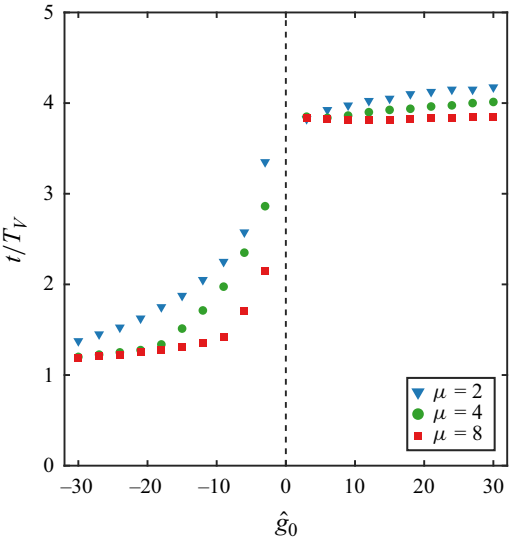

Figure 22. Time scale for transient adjustment where $\mu = 2$ ($\triangledown$), 4 ($\circ$) and 8 ($\square$).

of $h/H = 0.66,\ 0.44$ and 0.29, respectively. We assume the system has adjusted once the buoyancy profile is within 1 % of the final steady-state profile.

The simulations to the left of the vertical dashed line correspond to cases in which there is a reduction in the buoyancy of the air supply. For $g_0 < 0$, the adjustment time decreases as the buoyancy decreases, first quickly in the region $-15 \lesssim g_0 < 0$, then more slowly for $g_0 \lesssim -15$. We can explain this trend based on the dominant behaviour of the system. For small decreases, the original upper layer (a) is rapidly ventilated, but the original lower layer (b) is entrained into the plume much more slowly. In this region, there is a strong dependence on the degree of ventilation because as μ increases, the interface is lower and less fluid needs to be entrained, leading to a faster adjustment. For large decreases, the plume intrudes at a low level, and the ventilation drains all of the higher layers. In this region, the adjustment time is approximately proportional to the ventilation time scale because the rate-limiting step is the time taken to advect fluid up to the ceiling. The slight trend of decreasing adjustment time for larger decreases in buoyancy corresponds to the plume intruding sooner with a larger buoyancy reduction.

The simulations to the right of the dashed line correspond to increases in the buoyancy of the air supply. To first order, the adjustment time is proportional to the ventilation time scale where $t \approx 4T_V$. However, there is a small increase in the time scale with decreasing μ or increasing $\hat{g}_0$. This is because decreasing μ directly increases the volume of the original lower layer (1.2), and mixing a larger volume of fluid slows down the system evolution. In the lower-layer mixing regime ($\hat{g}_0 < \mu$), increasing $\hat{g}_0$ does not change the volume of the mixing zone, so there is no change to the adjustment time. However, in the total mixing regime ($\hat{g}_0 > \mu$), the layers will overturn sooner when the buoyancy of the supply is larger. As a result, less fluid has been transported to the ceiling in the plume, so the stratified layer (c) is smaller, and the mixing zone ($a + b$) is larger than for a less extreme change.

Commercial buildings often have ventilation time scales of 10–20 min. Based on our models, transient effects may be significant for one to two ventilation time scales when the temperature of the air supply is decreased and for four when the temperature of the air supply is increased. In these spaces, it may therefore be important to include the impact of transients in the design of the ventilation.

9. Conclusions

We have explored the effect of rapid changes to the temperature of the air supply on displacement ventilation. In steady state, the interaction of buoyant plumes rising from heat sources and the net upward ventilation flow leads to a two-layer stratification. But following a change in the temperature of the air supply complex, multi-layer, transient ventilation flows develop with significant impacts on air quality and comfort. We have identified four new transient flow regimes depending on whether the supply air is heated or cooled and the magnitude of this change in temperature relative to the temperature difference between the original two layers. A regime diagram, based on the degree of ventilation, μ, and the dimensionless temperature change, $\hat{g}_0$, is consistent with our new experiments. We have also proposed models for the flow evolution in each regime. Although this modelling is idealised, it captures the key features of the flow and, to leading order, provides a reasonable description of the experimental results.

Overall, the significance of any temperature variation must be considered from the reference frame of the building of interest. Large spaces typically have longer ventilation time scales, so temperature variations are more likely to approximate a step change. In addition, weak heat sources produce smaller temperature differences in the stratification, so a smaller temperature change can significantly change the dynamics. Therefore, we expect variations in the supply air temperature to be most significant for large buildings with relatively weak heat sources and least significant for small buildings with large heat loads.

As a simple application of this work, we consider the effect of these transient flows on contaminant dispersal in a building. In steady state, upward displacement ventilation is designed so that contaminants co-emitted with the heat source are transported into the upper layer, leaving a lower layer of fresh supply air. This study identifies that this principle does not always apply during transient ventilation flows. For example, the transients associated with cooling the air supply lead to an intrusion below the steady-state interface depth and a lateral spreading of air from the plume. Furthermore, warming the air supply leads to a mixing regime where occupants below the interface may be exposed to contaminants that were previously confined to the upper layer, albeit at a lower concentration. In certain spaces, changing occupancy patterns may lead to transients dominating the overall ventilation flow, and relying on the design of the steady state cannot accommodate these transient effects. We intend to examine transient contaminant transport in more detail, particularly for applications relating to disease transmission.

Declaration of interests. The authors report no conflict of interest.

Appendix A. Momentum condition

To examine the effect of the plume momentum flux on whether a plume will intrude, we can solve the plume equations analytically for a negatively buoyant plume (Morton & Middleton 1973). Assuming that the layer is uniform, (4.8) can be written as

$$\frac{\mathrm{d}m}{\mathrm{d}q} = -\frac{4}{5}\frac{|f_s|\,q}{m^{3/2}}. \tag{A1}$$

With the initial conditions $q = q_s$, $m = m_s$, $f = f_s < 0$ at $\xi = \xi_s$, this has a parametric solution:

$$q = \left(\frac{m_s^{5/2} - m^{5/2}}{|f_s|} + q_s^2\right)^{1/2} \tag{A2}$$

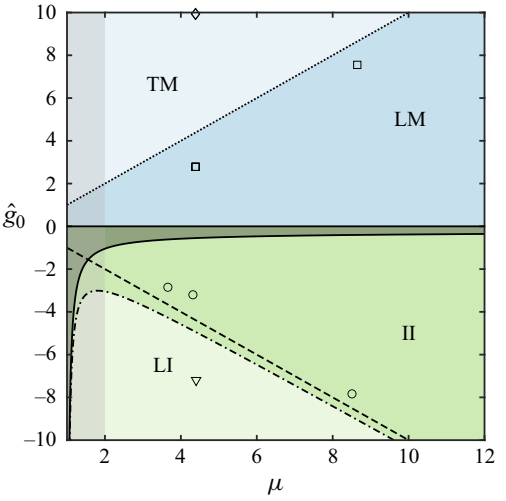

Figure 23. Regime diagram for the transient flows following a step change in the temperature of the air supply in terms of the size of the temperature change, $\hat{g}_0$, and the degree of ventilation, μ. Two new curves not present in figure 10 have been plotted. The solid curve separates flows with enough momentum to reach the ceiling from the intermediate intrusion regime (II) and the dashed-dotted line separates intermediate intrusions and low-level intrusions also accounting for the momentum flux of the plume. The symbols correspond to experiments where intermediate intrusions (○), low-level intrusions (▽), lower-layer mixing (□) or total mixing (◇) were observed.

leading to

$$\frac{\xi - \xi_s}{\ell_m} = \int_{\hat{m}}^{1} \frac{\hat{m}}{\left(1 - \hat{m}^{5/2} + |\Gamma_s|\right)^{1/2}} \, \mathrm{d}\hat{m}, \tag{A3}$$

where ξ is the height reached by the plume, $\hat{m} = m/m_s$ is a scaled momentum flux,

$$\ell_m = \frac{m_s^{3/4}}{|f_s|^{1/2}} \quad \text{and} \quad \Gamma_s = \frac{q_s^2 f_s}{m_s^{5/2}}. \tag{A4}$$

If we assume that the negatively buoyant plume source is produced by a pure plume crossing a density interface from a layer of negatively buoyant fluid into a layer with zero buoyancy, we can rewrite these parameters in terms of the layer depth ξ_c and buoyancy $\hat{g}_c$:

$$\ell_m = \frac{\xi_c}{\left|1 + \hat{g}_c \xi_c^{5/3}\right|^{1/2}} \quad \text{and} \quad \Gamma_s = f_s = \left|1 + \hat{g}_c \xi_c^{5/3}\right|. \tag{A5}$$

To obtain a momentum-based criterion for the low intrusion regime boundary, we explore the hypothesis that this requires the momentum to fall to zero at the the ceiling, $\hat{m} = 0$ at $\xi = 1$.

In general, the case of a non-zero density above an interface can be transformed into the zero-density case by the transformation $\hat{g}_1 \to \hat{g}_1 - \hat{g}_3(\xi, \tau)$ where, in general, $\hat{g}_3(\xi, \tau)$ will be a function of both the initial interface depth and time.

We consider the hypothetical scenario where the new lowest layer has entirely replaced the lower layer, but the composition of the upper layer has not changed. This leads to a modified length scale and plume parameter:

$$\ell_m = \frac{\xi_s}{\left|\hat{g}_1 \xi_s^{5/3}\right|^{1/2}} \quad \text{and} \quad \Gamma_s = f_s = \left|\hat{g}_1 \xi_s^{5/3}\right|. \tag{A6}$$

These results have been plotted using dashed lines in figure 23. Accounting for the momentum flux of the plume, we require a larger buoyancy change.

References

Alajmi, A. & El-Amer, W. 2010 Saving energy by using underfloor-air-distribution (UFAD) system in commercial buildings. *Energy Convers. Manage.* **51** (8), 1637–1642.

Baines, W.D. & Turner, J.S.S. 1969 Turbulent buoyant convection from a source in a confined region. *J. Fluid Mech.* **37** (1), 51–80.

Baines, W.D., Turner, J.S. & Campbell, I.H. 1990 Turbulent fountains in an open chamber. *J. Fluid Mech.* **212** , 557–592.

Bloomfield, L.J. & Kerr, R.C. 2000 A theoretical model of a turbulent fountain. *J. Fluid Mech.* **424**, 197–216.

Bolster, D. & Caulfield, C.-C.P. 2008 Transients in natural ventilation – a time-periodically-varying source. *Build. Serv. Engng Res. Technol.* **29** (2), 119–135.

Bolster, D.T. & Linden, P.F. 2007 Contaminants in ventilated filling boxes. *J. Fluid Mech.* **591**, 97–116.

Bower, D.J., Caulfield, C.P., Fitzgerald, S.D. & Woods, A.W. 2008 Transient ventilation dynamics following a change in strength of a point source of heat. *J. Fluid Mech.* **614**, 15–37.

Fitzgerald, S.D. & Woods, A.W. 2007 Transient natural ventilation of a room with a distributed heat source. *J. Fluid Mech.* **591**, 21–42.

Fitzgerald, S.D. & Woods, A.W. 2010 Transient natural ventilation of a space with localised heating. *Build. Environ.* **45** (12), 2778–2789.

Hunt, G.R. & Burridge, H.C. 2015 Fountains in industry and nature. *Annu. Rev. Fluid Mech.* **47**, 195–220.

Hunt, G.R. & Kaye, N.B. 2006 Pollutant flushing with natural displacement ventilation. *Build. Environ.* **41** (9), 1190–1197.

Kaye, N.B. & Hunt, G.R. 2004 Time-dependent flows in an emptying filling box. *J. Fluid Mech.* **520**, 135–156.

Kumagai, M. 1984 Turbulent buoyant convection from a source in a confined two-layered region. *J. Fluid Mech.* **147** (−1), 105.

Lane-Serff, G. 1989 Heat flow and air movement in buildings. *PhD thesis*, University of Cambridge, UK.

Lane-Serff, G.F., Linden, P.F. & Smeed, D.A. 1990 Laboratory and mathematical models of natural ventilation. *Room-Vent* **A2** (7), 1–7.

Lima Neto, I.E., Cardoso, S.S.S. & Woods, A.W. 2016 On mixing a density interface by a bubble plume. *J. Fluid Mech.* **802**, 1–13.

Lin, Y.J.P. & Linden, P.F. 2005*a* A model for an under floor air distribution system. *Energy Build.* **37** (4), 399–409.

Lin, Y.J.P.P. & Linden, P.F. 2005*b* The entrainment due to a turbulent fountain at a density interface. *J. Fluid Mech.* **542**, 25–52.

Linden, P.F. 1999 The fluid mechanics of natural ventilation. *Annu. Rev. Fluid Mech.* **31** (1), 201–238.

Linden, P.F., Lane-Serff, G.F. & Smeed, D.A. 1990 Emptying filling boxes: the fluid mechanics of natural ventilation. *J. Fluid Mech.* **212**, 309–335.

Liu, Q.A. & Linden, P.F. 2006 The fluid dynamics of an underfloor air distribution system. *J. Fluid Mech.* **554**, 323–341 .

Mcdougall, T.J. 1981 Negatively buoyant vertical jets. *Tellus A: Dyn. Meteorol. Oceanogr.* **33** (3), 313.

Morton, B., Taylor, G. & Turner, J. 1956 Turbulent gravitational convection from maintained and instantaneous sources. *Proc. R. Soc. Lond.* **234** (1196), 1–23.

Morton, B.R. & Middleton, J. 1973 Scale diagrams for forced plumes. *J. Fluid Mech.* **58** (1), 165–176.

Savardekar, K. 1990 Aspects of passive cooling: a study on natural ventilation. *PhD thesis*, University of Cambridge, UK.

Toy, D.A. & Woods, A.W. 2025 The impact of natural convection and turbulent mixing on mechanical ventilation. *J. Fluid Mech.* **1002**, A7.